Digital Predistortion of Wideband Satellite Communication Signals with Reduced Observational Bandwidth and Reduced Model Order Complexity

Pedro Miguel Brinco de Sousa
pedro.brinco.de.sousa@tecnico.ulisboa.pt

Instituto Superior Técnico, Lisboa, Portugal

November 2014

Abstract

The increase in the demand for wireless communications from the user-end point of view calls for an infrastructure that is constantly more capable, reliable and efficient. One of the critical nodes in the telecommunications process, from the hardware perspective, is the power amplifier (PA): it is not only the more power-consuming device in the transmission chain but it also has a highly nonlinear behaviour which can compromise the well-functioning of the communications infrastructure. This thesis addresses the digital predistortion (DPD) technique, whose goal is to reduce the nonlinear influence of the PA in the transmitted signal, and enhances it with two contributions which can allow for a bigger computational and economic efficiency without compromising the effectiveness of DPD. These contributions are the Reduced Observational Bandwidth and the Reduced Model Order. In the former, the observational path required for the implementation of the DPD is redesigned to permit the capture of wideband signals using multiple reduced bandwidth observations. The latter, on the other hand, aims at reducing the number of coefficients needed for DPD by discarding the less contributive modes of the PA behavioural model. Additionally, the technique of reducing the signal PAPR is applied in order to seek a more effective predistortion. The experimental campaign in a real DUT proved that the reduction of the observational bandwidth was feasible and produced similar results when compared to a full spectrum observation.

Keywords: satellite communications, power amplifier, linearisation, digital predistortion

1. Introduction

In the 21st century, telecommunications play a key-role in the daily-life of both people and companies. For example, in 2013, the revenues of the global telecommunications industry were reported to be of 5 billion U.S. dollars, having grown 7% since the previous year. Though representing only 4% of the total revenues, the majority of the satellite market depends, on the other hand, on the telecommunications business — 53% of the active satellites in 2013 have the sole purpose of governmental and commercial communications [1]. These figures are backed by an ever bigger and hunger market on a global scale. While the duty of the governing institutions is to improve the spectrum management [2], the companies are required to use their part of the spectrum more efficiently while obeying stricter sets of rules.

Therefore, the power amplifier (PA) presents itself as a critical point towards the accomplishment of the referred goals: it is the main source of nonlinearities present in the transmission chain. Furthermore, communications standards in use nowadays are usually synonym of high PAPR values. This means that the PA has to be driven very far from its ideal working conditions to be able to cope with the peaks of the signals without being saturated. In addition to the high PAPR values, the necessity of high data rates to cope with the traffic demand, leads to standards of telecommunications imposing greater bandwidths for the carriers: for example, the LTE carriers can have up to 20 MHz. This order of magnitude of the bandwidths, and which tends to increase, brings the necessity of high speed analogue-to-digital converters to recover the signal for processing, which is not cost-effective.Finally, the complexity of the PA behaviour usually requires a large and complex mathematical model to describe it. Due to the fact that the adaptation process is commonly related to a reduction of a quadratic error, the extraction of the coefficients relies on techniques such as the Least Mean Squares, which can benefit from the well-conditioning of the matrices.

2. Background

As referred in the introduction the PA is the main source of nonlinearities in the transmission chain. Ideally, the relation between the input and output signals of the PA would be represented just as a scalar gain. Let $v_{in}(t)$ be the input signal, then the output would be given by (1).

$$v_{out}(t) = g \cdot v_{in}(t), \tag{1}$$

where g is a scalar gain. However, and depending on the driving load of the PA, the PA is limited to a certain output power (Fig. 1) which causes this device to have a non-linear characteristic.

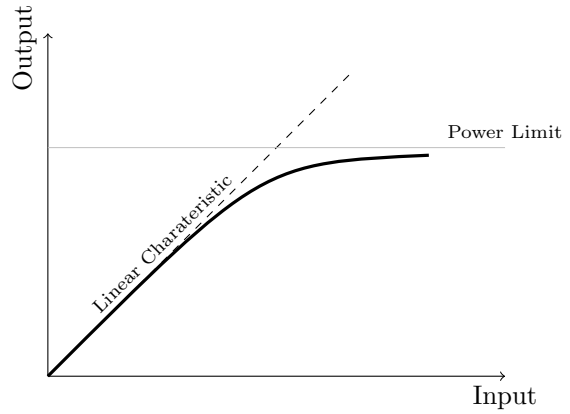

Figure 1: Real behaviour of a PA.

Therefore, it is proposed [3, 4] that over a limited range of $v_{in}(t)$ amplitude, the representation of the output of a PA can be given by the complex power series

$$v_{out}(t) \simeq \sum_{k=0}^{\infty} a_k . v_{in}^k(t), \tag{2}$$

where a_k is a gain which depends on the order k. For $k = 1$, this expression yields the same result as (1), that is, the linear term of the system. However, this model leads to the conclusion that newer terms will be introduced in the output signal apart from the amplification of the original input: *harmonics* in the multiples of the carrier frequency, generated by the even values of k, and *intermodulation products*, generated by the odd terms. Both these new components constitute distortion and while the former can be filtered out, intermodulation distortion may fall too close to the useful band of the signal to allow for a filtering to be carried out. A measure of the distortion due to the nonlinearities of the PA can be defined as the *Adjacent Channel Leakage Ratio* (ACLR):

$$ACLR = 10 \log \left(\frac{\int_{f_{adj}} |Y(f)|^2 df}{\int_{f_{chan}} |Y(f)|^2 df} \right), \tag{3}$$

where $Y(f)$ is the Fourier transform of $y(t)$ and f_{adj} and f_{chan} are the bandwidths of the adjacent channel in study (first higher, first lower, second higher, ...) and of the allocated channel, respectively. This quantity measures the amount of power that is being leaked to the adjacent bandwidths normalized by the total power of the signal in the channel.

Furthermore, the linearity of a power amplifier is closely tied to its efficiency. There are operating classes of the PA, such as the A, AB and C, in which the PA behaves as voltage-controled current source, thus being highly linear. On the other hand, in D, E and F classes, the PA behaves like a switch, thus achieving high efficiency, but having a poor linear behaviour [5]. This leads to the necessity of establishing a trade-off between linearity and efficiency.

Finally, the mathematical behaviour described by (1), does not account for memory effects which are usually present in the amplifier. These memory effects are usually due to the non-constant envelopes of the signal, to the temperature changes in the device, impedance variances, mismatches in the remaining circuitry and even in the power supply of the transistor [6]. These memory effects tend to be more discernible in wideband input signals [7].

3. Implementations

3.1. Digital Predistortion

There are numerous examples in literature to overcome the linearisation problem in the PA. These techniques can be classified as *circuit-level* if the linearisation is performed directly on the device and *system-level* if they approach the system, which includes the PA, as a whole. At the system-level, there are techniques such as Feedback, Feedforward and Envelope Elimination and Restoration. In addition, there is also predistortion, which consists in distorting the original signal in such a way that when amplified by the PA, the relation between the input and output becomes linear, as depicted in Figure 2.

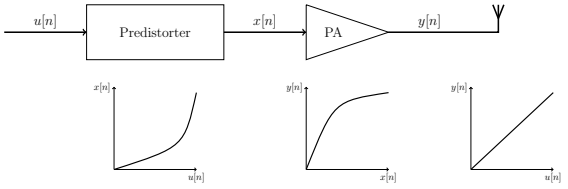

Figure 2: Principle of Predistortion.

The predistortion can be achieved with both analogue components or by means of digital processing, using DSP and FPGA. Therefore, digital predistortion of signals consists in a quite straightforward and common approach: the signal is sent through a predistorter which generates an output that will

feed the PA.

In order to build the predistorter, it is important to define the model that will numerically describe the PA. The proposed method is the *Memory Polynomial* method, which despite its simplicity, is enough to validate the algorithms that are used in this thesis. Hence, (2) is replaced by

$$\widehat{y}[n] = \sum_{k=1}^{M} \sum_{p=1}^{P} a_{kp}.\gamma_{kp}[n], \tag{4}$$

where a_{kp} are the model coefficients and γ_{kp} is called the *basis waveform* [8] which is defined as

$$\gamma_{kp}[n] = x[n-\tau_k].\left|x[n-\tau_k]\right|^{p-1}, \tag{5}$$

where τ_k is the k^{th}-component of the delay vector $\underline{\tau}$ that can be defined as

$$\underline{\tau} = \begin{bmatrix}\tau_1 & \tau_2 & \dots & \tau_M\end{bmatrix}. \tag{6}$$

The components of $\underline{\tau}$ are called *memory taps* and τ_1 usually corresponds to the non-delayed contribution of the input, that is $\tau_1 = 0$. Equation 4 can be rewritten in matrix form as

$$\underline{\hat{y}} = F_x \underline{a}, \tag{7}$$

where the vectors $\underline{\hat{y}}$ and $\underline{a}$ and the matrix F_x are given by

$$\underline{\hat{y}} = \begin{bmatrix}\hat{y}(0) & \hat{y}(1) & \dots & \hat{y}(S-1)\end{bmatrix}^T, \tag{8}$$

$$\underline{a} = \begin{bmatrix}a_{11} & a_{12} & \dots & a_{MP}\end{bmatrix}^T, \tag{9}$$

$$F_x = \begin{bmatrix}\underline{f_{11}} & \underline{f_{12}} & \dots & \underline{f_{MP}}\end{bmatrix}, \tag{10}$$

where S is the number of samples and $\underline{f_{kp}}$ is defined as

$$\underline{f_{kp}} = \begin{bmatrix}\gamma_{kp}(0) & \gamma_{kp}(1) & \dots & \gamma_{kp}(S-1)\end{bmatrix}^T. \tag{11}$$

The subscript x in the matrix F_x denotes that the basis waveforms used to construct the matrix are generated using the input signal $x[n]$. The coefficients $\underline{a}$ can be obtained using the Least Squares method, whose solution is given by

$$\underline{a} = \left(F_x^H F_x\right)^{-1} F_x^H \underline{\hat{y}} \tag{12}$$

where $(.)^H$ denotes the conjugate transpose of the matrix F.

Extracting the coefficients using (12) generates coefficients that prove adequate over a narrow band of operating conditions [7]. It is necessary to make this estimation adaptive in order to extend this band of operating conditions in which the coefficients are adequate.

The first method is called the *direct method* (Fig. 3) and it is based in defining the error as

$$e[n] = y[n]G_0^{-1} - u[n], \tag{13}$$

where G_0 is the linear gain of the PA. Therefore, and knowing the PA output, the coefficients can be computed iteratively using a weighted Least Squares method defined as

$$\underline{\Delta a_i} = \left(F_u^H F_u\right)^{-1} F_u^H \underline{e}, \tag{14}$$

$$\underline{a_{i+1}} = \underline{a_i} + \lambda \underline{\Delta a_i}, \tag{15}$$

in which F_u is constructed with basis waveforms generated from $u[n]$, $\underline{\Delta a_i}$ is the coefficients vector computed at the i^{th}-iteration and the weight factor λ is a value between 0 and 1. The additive distortion $d[n]$ caused by the PA can be applied to the input signal as

$$d[n] = F_u \underline{a_i}, \tag{16}$$

and, therefore, the new PA input is described by the predistorter relation as

$$x[n] = u[n] - d[n]. \tag{17}$$

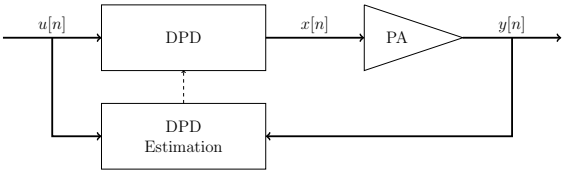

Figure 3: Direct Learning method for DPD.

On the other hand, the error can be defined as

$$e[n] = \widehat{x}[n] - x[n], \tag{18}$$

which leads to the *indirect method* (Fig. 4). The postdistorted estimated output can be obtained using the relation

$$\widehat{d}[n] = F_y \underline{a_i}, \tag{19}$$

where F_y is a matrix whose basis waveforms γ are constructed using the output signal $y[n]$. The estimated PA input is defined as

$$\widehat{x}[n] = y[n]G_0^{-1} - \widehat{d}[n], \tag{20}$$

which allows, by using Equation (18), to compute the error. As with the direct method, the error is used to estimate iteratively the coefficients using

$$\underline{\Delta a_i} = \left(F_y^H F_y\right)^{-1} F_y^H \underline{e}, \tag{21}$$

and

$$\underline{a_{i+1}} = \underline{a_i} + \lambda \underline{\Delta a_i}. \tag{22}$$

Afterwards, both Equations (16) and (17) can be used to compute the new PA input.

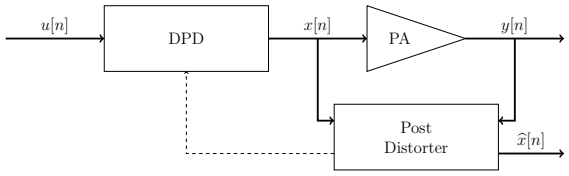

Figure 4: Indirect Learning method for DPD.

3.2. PAPR Reduction

It is possible to define a Figure of Merit that characterizes the relation between the peak and the mean value of a signal — the *Peak-to-Average Power Ratio* (PAPR).

$$PAPR = 10 \log \left(\frac{P_{peak}}{P_{avg}} \right), \tag{23}$$

The signals in use for telecommunications nowadays have a high level of PAPR. This compromises the efficiency of the PA by compressing the output if one wishes to drive the PA as close to saturation as possible. Therefore, a reduction of the PAPR is usually performed to the input signal $u[n]$ before using it in the digital predistortion algorithm. The proposed technique to reduce this FoM is called *Scaled Peak Cancellation* (SPC) [9]. Let the clipper pulse $c[n]$ be defined as

$$c[n] = \begin{cases} \frac{A}{\left|u[n]\right|} & \text{if } \left|u[n]\right| > A \\ 1 & \text{if } \left|u[n]\right| \leq A \end{cases}, \tag{24}$$

where A is the suppressing threshold. The clipped pulse $p[n]$ is, then, defined as

$$p[n] = u[n] - u[n] \cdot c[n]. \tag{25}$$

The output of this clipped pulse has to be filtered with a low-pass filter with the same bandwidth as that of the $u[n]$. If $u[n]$ is multi band signal, each band has to be filtered individually and then recombined. The PAPR-reduced signal $z[n]$ is finally obtained with

$$z[n] = u[n] - \alpha \cdot p[n] * h[n], \tag{26}$$

where $h[n]$ is the impulse response of the filter, $*$ denotes the convolution operation and α is a weight factor defined as

$$\alpha = \frac{max\left(\left|p[n]\right|\right)}{max\left(\left|p[n] * h[n]\right|\right)}. \tag{27}$$

This technique can be implemented repetitively by making $u[n] = z[n]$ at the end of each iteration, leading to a technique called *Repeated Peak Cancellation* (RPC). The drawback of this technique is distorting the information that is contained in the original signal. Hence, a trade-off has to be guaranteed between reducing the PAPR and maintaining the integrity of the signal.

3.3. Reduced Observational Bandwidth

One of the main components of the feedback path in the DPD context is the *Analogue-to-Digital Converter*, commonly referred to as ADC. The role of the ADC is to convert the analogue signal, that is recovered through the feedback path, to a digital signal that can be processed. One of the main characteristics of the ADC is the sampling rate, which is the rate at which the samples of the analogue signal are captured and converted to digital. The *Shannon-Nyquist Theorem* states that if a signal has no frequencies higher than B_0 hertz, then it will be completely represented by samples captured $1/(2B_0)$ seconds apart [10]. The analysis of this problematic leads to the conclusion that, in order to represent wide bandwidth signals with all their intermodulation products, there is a call for an ADC with a sampling rate, at least, twice as big as the signal bandwidth.

In order to reduce the bandwidth of a signal, it is proposed [11] a form of capturing the signal which consists in using an *observational window* which has a bandwidth B_{obs} that is smaller than the signal bandwidth. In order to avoid the loss of information that would arise by simply limiting the signal, the effective captured bandwidth is increased by up and down converting the signal at different frequencies so as the area of the spectrum covered by the observational window is different. The use of these different observations allows for the signal to be reconstructed in the digital domain, relieving the ADC from sampling at high rates. The principle is depicted in Figure 5 and combines a tunable local oscillator (LO) followed by a low-pass filter whose bandwidth is B_{obs} before the signal is sent to the ADC. The LO is tuned in order to demodulate the original signal so as the centre of the observational window is the same as the filter's.

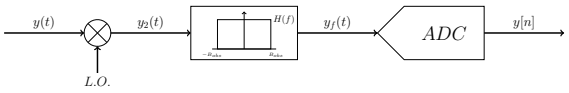

Figure 5: Scheme of the reduced observational bandwidth windowing technique.

The reconstruction of the signal in the digital domain starts with a demodulation of each set to baseband, which can be substituted by a simply fre-

quency shift. After the signal is demodulated to baseband, an ideal filtering can be performed to filter out the window more effectively. Following that, there is a necessity to align each spectrum to its correct position. The knowledge of the centre frequency of each window reduces this problem to a simple shift of each set to the frequency of its corresponding window. In Figure 6 an example of five observational sets of 30 MHz each is depicted after alignment.

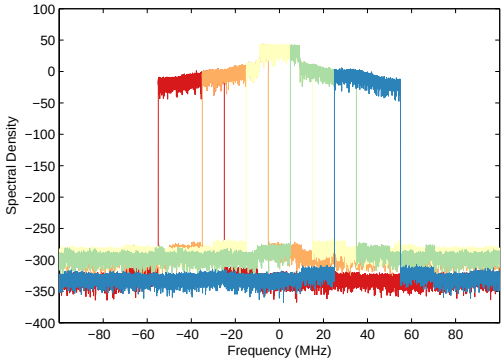

Figure 6: Five observational windows of 30MHz each, covering an effective bandwidth of 110MHz, after alignment.

The last step of reconstruction is the merger of the various observations into one signal, which is the reconstructed output. Although it is a straightforward process because it only implies picking the relevant part of the spectrum from each observation, the ideal filtering that was previously made creates a discontinuity in the filter cut-off frequency that has to be avoided when picking the spectrum. This issue is overcome, firstly, by guaranteeing that the windows overlap each other when projecting the system, and then by applying an algorithm that discards the last samples of the window when picking. The recovered signal is depicted in Figure 7.

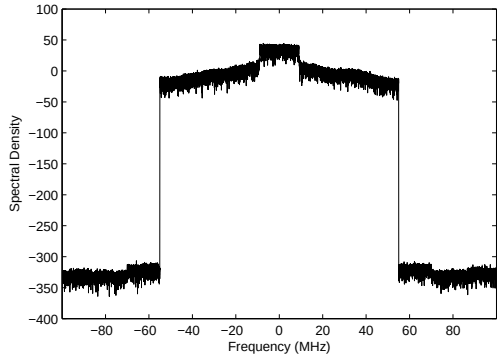

Figure 7: Recovered signal after reconstruction.

Finally, and in order to take advantage of the fact that the signal was recovered in the frequency domain, the estimation can be done without converting the signal to the time domain [8]. Let the Fast Fourier Transform (FFT) of the basis waveform presented in (5) be defined as:

$$\Gamma_{kp}(\omega_n) = \mathcal{FFT}\left\{\gamma_{kp}[n]\right\}. \tag{28}$$

Therefore, the vector f and the matrix F can be redefined as ψ and Ψ, respectively, where:

$$\underline{\psi_{kp}} = \begin{bmatrix}\Gamma_{kp}(\omega_0) & \Gamma_{kp}(\omega_1) & \dots & \Gamma_{kp}(\omega_{S-1})\end{bmatrix}^T, \tag{29}$$

and

$$\Psi_x = \begin{bmatrix}\underline{\psi_{11}} & \underline{\psi_{12}} & \dots & \underline{\psi_{MP}}\end{bmatrix}. \tag{30}$$

Consequently, the construction of matrix Ψ is equivalent to applying the FFT along the columns of matrix F. However, in order to reduce the complexity of the FFT, the number of samples should be short and, preferably, a power of 2. The matrix Ψ is, then, constructed by applying the FFT to various sets of samples and averaging them.

The LMS solution in the frequency domain becomes

$$\underline{a} = \left(\Psi_x^H \Psi_x\right)^{-1} \Psi_x^H \underline{Y}, \tag{31}$$

where $\underline{Y}$ is the output in the frequency domain. Therefore, an adaptive process can also be constructed, similarly to what has been done for the direct method for example. By applying the same concept of sets of samples to the input $u[n]$, it is possible to define $U(\omega_n)$ as

$$U(\omega_n) = \mathcal{FFT}\left\{u[n]\right\}, \tag{32}$$

which allows for the computation of the error in the frequency domain as

$$E(\omega_n) = Y(\omega_n)G_0^{-1} - U(\omega_n), \tag{33}$$

taking advantage of the fact that $y[n]$ was extracted in the frequency domain. Hence, by applying the FFT along the columns of the matrix F_u to obtain the matrix Ψ_u, such as described above, the weighed LMS solution becomes

$$\underline{\Delta a_i} = \left(\Psi_u^H \Psi_u\right)^{-1} \Psi_u^H \underline{E}, \tag{34}$$

3.4. Model Order Reduction

In both direct and indirect methods, a matrix F — or the matrix Ψ in the frequency estimation — was constructed from the basis waveforms γ generated from the signal which is used as the input in each method. The size of the matrix F is $S \times N$, regardless of the learning method used, and where S is the number of samples used to determine the model and N the number of coefficients. However,

the number of coefficients used for the model has an effect on the accuracy of the model estimation. Therefore, a low ratio is desirable, with experimental results supporting a number of samples that is, at least, 20 times the number of coefficients [12].

Principal Component Analysis (PCA) [13] is a statistical technique which allows for the reduction of the dimensions of a given set of variables by orthogonally transforming the original, and possibly correlated, variables into an uncorrelated set, the *principal components*. These principal components are ordered in such a way that the variance decreases along them which leads to the fact that the first few components account for almost the totality of the variance present in all set [14].

Therefore, it is necessary to define the empirical covariance matrix of F as

$$cov(F) = F^H F, \tag{35}$$

where $(.)^H$ denotes the conjugate transpose of the matrix F. This square matrix can be factorized using eigendecomposition, resulting in

$$cov(F) = V \Lambda V^{-1}, \tag{36}$$

in which Λ is a diagonal matrix containing the eigenvalues of the covariance matrix and V a matrix consisting of the corresponding eigenvectors. The orthogonal transformation can, then, be defined as

$$\widetilde{F} = FV, \tag{37}$$

where the columns of $\widetilde{F}$ are the principal components of F. However, it is possible to discard some of the basis in which the variance is small while preserving the basis with larger variance. Therefore, we can truncate the matrix V up to L vectors, with $L < N$, and still retain the majority of the variance of the data. The orthogonal relation of (37) can be rewritten as

$$\widetilde{F} = FV_L, \tag{38}$$

where V_L is the truncated matrix, and which leads to a matrix $\widetilde{F}$ of size $S \times L$, therefore reducing the number of coefficients that will be outputted to L.

4. Results

Testing in a DUT offers a significant advantage when compared to numerical simulations: a model used to describe the PA is a limited model in the sense that it does not cover perfectly the dynamic range in which the PA was not tested to when the model was obtained. The experimental set-up follows the schematic depicted in Figure 8.

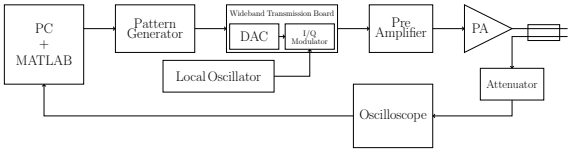

Figure 8: Diagram of the set-up used in the experimental campaign.

The Reduced Observational Bandwidth method aims to feed the ADC with sets of narrow bandwidth observations to be converted to the digital domain and used later to reconstruct the original signal. However, as it can be seen by Figure 8, the set-up does not have an ADC. Instead, the signals are converted by sampling in the oscilloscope. Therefore, in order to test the algorithm, the solution was to emulate an ADC, using the algorithm depicted in Figure 9.

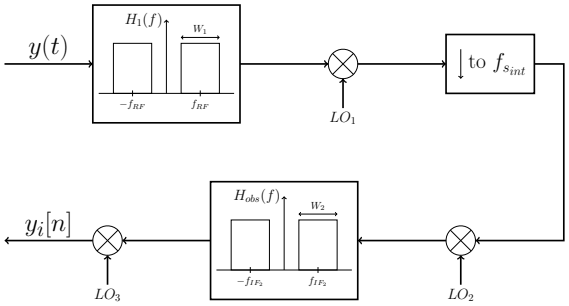

Figure 9: Schematic representation of the algorithm used to emulate an ADC.

The local oscillators frequencies are given by:

$$f_{LO_1} = f_{RF} - f_{IF_1}, \tag{39}$$

$$f_{LO_2} = f_{IF_1} - f_{IF_2} + f_{w_i}, \tag{40}$$

$$f_{LO_3} = f_{IF_2} + \frac{W_2}{2}. \tag{41}$$

The intermediate frequencies have to be chosen carefully in order to avoid that during the various demodulations,an overlap occurs between the replicas created due to the cosine multiplications. Therefore, these frequencies are a function of the first filter bandwidth W_1 and of the highest observational window centre frequency. This question can be solved algorithmically, and by having W_1 as 240 MHz and with a maximum centre of the observational windows being 90 MHz, the solutions are

$$f_{IF_1} = 450 \text{ MHz}, \tag{42a}$$

$$f_{IF_2} = 230.4 \text{ MHz}. \tag{42b}$$

The last parameters to be analysed are the frequency rates $f_{s_{int}}$ and $f_{s_{ADC}}$ which were defined to be 2 GHz and 61.44 MHz, respectively.

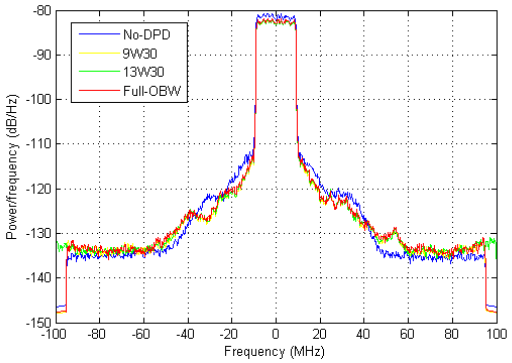

(a) Single LTE signal.

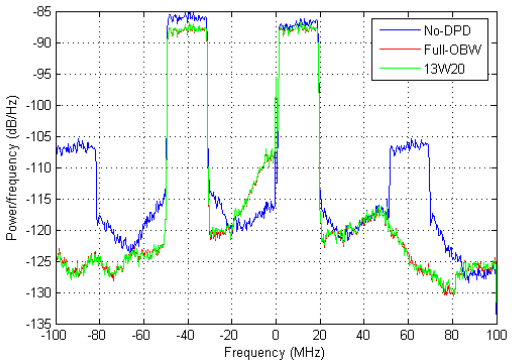

(b) LTE-CA signal.

Figure 10: Graphical output of the Reduced Observational Bandwidth performance test.

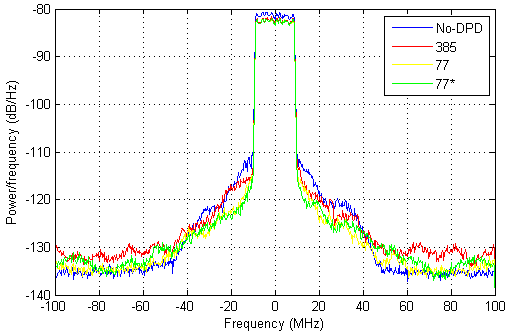

(a) Single LTE signal.

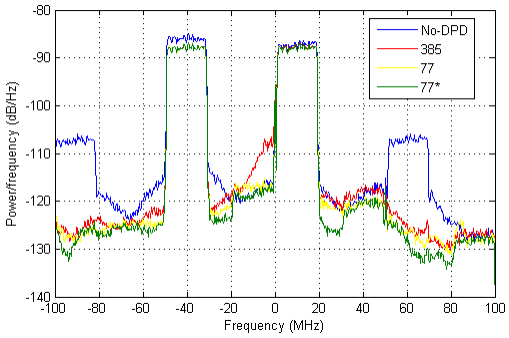

(b) LTE-CA signal.

Figure 11: Graphical output of the Model Order Analysis test.

The signals that were used for this experimental campaign were OFDM-based signals. It was used a single LTE signal, with 20 MHz of bandwidth, and a LTE-CA signal in which the LTE signal was replicated at -40.2 MHz and at 10.2 MHz. These frequencies comply with the carrier aggregation standards for LTE.

The first experiment tested the performance of the reduced observational bandwidth in both a single LTE (Fig. 10(a)) and a multiband LTE-CA signal (Fig. 10(b)). Signals were recovered using the full spectrum, and also using reduced observations (13 windows of 20 MHz and 9 windows of 50 MHz). It is possible to conclude that the predistortion technique using frequency estimation is not very effective in the single band test, as opposed to the dual-band where it reduced the intermodulation products. Furthermore, the change in the size of the windows tested in the single-band case returned similar results and the reduced observational bandwidth and the full-observational bandwidth also returned similar results in both tests. Finally, the dual-band scenario suffers from distortion created in the I/Q modulator which leads to the existence of uncorrected areas (between -20 and 0 MHz and between around 25 MHz and 45 MHz).

The second test (Fig. 11) addressed the influence of the model order in the predistortion. In comparison was the same recovery method using 385 coefficients (polynomial of order 11 and 35 memory taps) and 77 coefficients (order 7 and 11 memory taps). An extra comparison was made by reducing the model order by a factor of 5, that is, the original 385 were reduced to 77, denoted in the results by *77**. In this experiment, the tests in which a lower order was used, the DPD proved to be more effective in both signals. Additionally, in the dual-band scenario, the *77** test performed better than the *77*, mainly by reducing the leakage in the adjacent bands of the carriers.

In the following test, the LTE signal (Fig. 12(a)) and the LTE-CA (Fig. 12(b)) were submitted to DPD estimation in both time (using the direct learning method) and in frequency. In both cases, there was also considered the model-order reduction with a factor of 20 for comparison. Therefore, the number of coefficients used was 385 (polynomial of order 11 and 35 memory taps) and the reduction led to 19 coefficients, denoted as *19**. The first thing to be noted in the single LTE test is that the *F-385* case does not prove very effective when compared to the situation without DPD. The

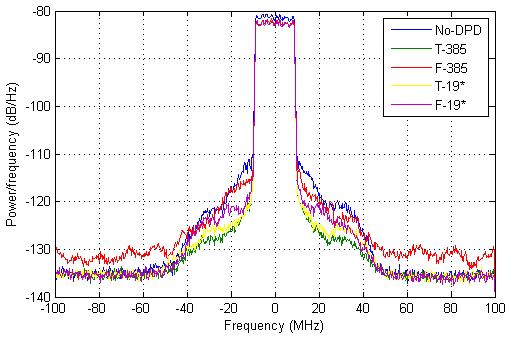

(a) Single LTE signal.

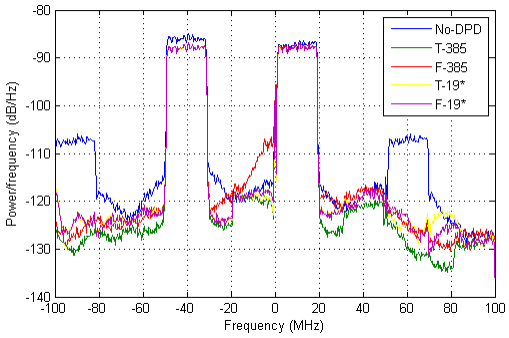

(b) LTE-CA signal.

Figure 12: Graphical output of the Time *vs.* Frequency-estimation test.

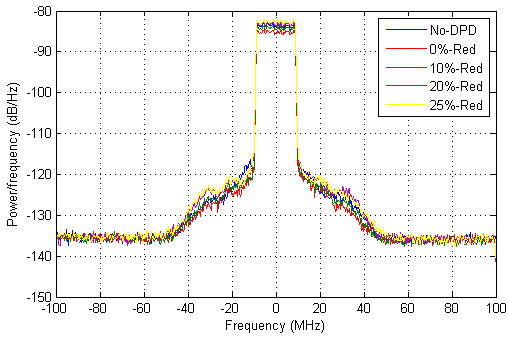

(a) Single LTE signal.

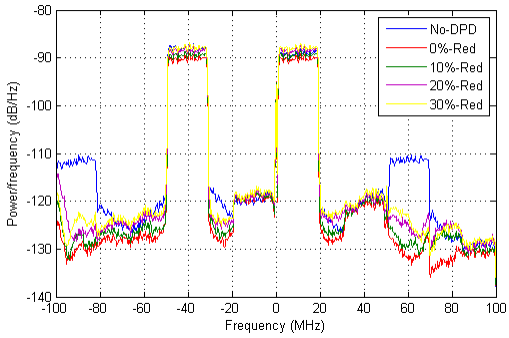

(b) LTE-CA signal.

Figure 13: Graphical output of the influence of PAPR in DPD.

other three scenarios effectively reduced the ACLR values, in special the time-estimated cases which reached 6-7 dB improvement in the first sideband ACLR and more than 3 dB in the NMSE. In the LTE-CA case, despite all scenarios having improved the total bandwidth leakage, the *F-385* did not improve the intra-carrier leakage. As mentioned in the previous tests, this case proved to be sensitive to the I/Q imbalance, thus leading to a degradation of the referred ACLR. To sum up, the time-estimated scenarios provided a better DPD performance than the frequency-estimated ones, either with a complete set of coefficients or with a reduced set.

In the last part of the testing (Fig. 13), it was sought to compare the response of the DPD when the signal was subjected to the PAPR reduction technique. There were used 385 coefficients (polynomial of order 11 and 35 memory taps) which were reduced by a factor of 20, yielding 19 coefficients. The results for this test have to be analysed more carefully. In fact, only the No-DPD and 0%-reduction cases can be compared directly in terms of ACLR and NMSE because they correspond to the same situation. All other cases would have to be compared to the No-DPD case in which the same reduction factor would have been applied. In the Single LTE test, PAPR reduction did not prove to be an improvement when compared to the case where no PAPR reduction was applied. In the LTE-CA case, all solutions proved effective in reducing the ACLR when compared to the No-DPD case. In this test, the case in which no reduction was applied presented better results, at the expense of a lower power. Therefore, a trade-off may have to be considered between the reduction of ACLR desired and the power output.

5. Conclusions

The tests that were performed did not prove to be very rewarding scientifically, as the results obtained did not meet some of the expectations that existed when the thesis started. This is mainly due to the fact that fine adjustments had to be made in the digital predistortion process in order to overcome system issues, such as the imbalance in the I/Q. Nonetheless, all the topics covered in this dissertation were put to test and some conclusions can be drawn from the experimental campaign.

First of all, reducing the observational bandwidth of a signal for its capture has been proved to be as DPD efficient as when the full spectrum of the signal is recovered. In addition, the method also returned similar results using different observational bandwidths, provided that the effective area covered by all sets of bandwidths is the same.

Secondly, the model order reduction returned better or similar results, but only in the frequency-estimation method. In the time-domain estimation, the full-order model proved to be more efficient.

Moreover, the estimation in frequency did not prove to be as effective as the estimation in the time-domain. This can be linked to the inefficiency described above for the model-order reduction. The results obtained with time-domain estimation returned better results than those obtained with frequency estimation. However, a more complete analysis relating the performance of these two methods together with the model order would have to be performed in order to establish the degree of dependence of each methods with the number of coefficients. In addition, the high order frequency-based estimation proved inefficient in overcoming the imbalances caused by the I/Q modulator that interfered with the signal.

Finally, a direct correlation between the reduction of the PAPR and the efficiency of the DPD could not be found. Despite this fact, the PAPR was reduced up to 75% of its original value and still an improvement on the ACLR values was verified when compared to the case where no reduction and no DPD were performed. Therefore, and without compromising the integrity of the signals, the DPD was proven to be able to perform in PAPR-reduced signals.

Acknowledgements

The author would like to thank his supervisor in the UPC, Pere L. Gilabert, as well as his supervisor in the IST, António Rodrigues. This acknowledgement is extended to the personnel and colleagues in the TSC department of UPC, as well as, the colleagues in the MAST and in the Aerospace Engineering courses. Finally, the author would like to thank the support and dedications given to him by his family and friends.

References

[1] The Tauri Group. State of the Satellite Industry Report. Technical report, Satellite Industry Association, May 2014.

[2] Telecommunications Industry Association. TIA 2014 Playbook. Technical report, Telecommunications Industry Association, Arlington, VA, USA, 2014.

[3] Jos Carlos Pedro and Nuno Borges Carvalho. *Intermodulation Distortion in Microwave and Wireless Circuits*. Artech House, 2003. ISBN: 1580533566.

[4] Dominique Schreurs, Mirtn O'Droma, Anthony A. Goacher, and Michael Gadringer. *RF Power Amplifier Behavioral Modeling*. The Cambridge RF and Microwave Engineering Series. Cambridge University Press, 2009. ISBN: 9780521881739.

[5] Abdulrhman Mohammed Salman Ahmed. *Analysis, Modelling and Linearization of Nonlinearity and Memory Effects in Power Amplifiers Used for Microwave and Mobile Communications*. PhD thesis, University of Kassel, Germany, March 2005. ISBN: 9783899581461.

[6] Joel Vuolevi and Timo Rahknonen. *Distortion in RF Power Amplifiers*. Artech House, 2003. ISBN: 1580535399.

[7] R. Neil Braithwaite. Principles and Design of Digital Predistortion. In Fa-Long Luo, editor, *Digital Front-End in Wireless Communications and Broadcasting — Circuits and Signal Processing*, chapter 6. Cambridge University Press, 2011. ISBN: 9781107002135.

[8] R. Neil Braithwaite. Model order selection for digital predistortion of a rf power amplifier when the distortion spectrum exceeds the observation bandwidth. *International Journal of Microwave and Wireless Technologies*, 5:163–170, April 2013.

[9] Wan-Jong Kim, Kyoung-Joon Cho, ShawnP. Stapleton, and Jong-Heon Kim. An efficient crest factor reduction technique for wideband applications. *Analog Integrated Circuits and Signal Processing*, 51(1):19–26, 2007.

[10] C.E. Shannon. Communication in the presence of noise. *Proceedings of the IEEE*, 86(2):447–457, Feb 1998.

[11] R.N. Braithwaite. Wide bandwidth adaptive digital predistortion of power amplifiers using reduced order memory correction. In *Microwave Symposium Digest, 2008 IEEE MTT-S International*, pages 1517–1520, June 2008.

[12] Ali Soltani Tehrani. *Behavioral modeling of wireless transmitters for distortion mitigation*. PhD thesis, Chalmers University of Technology, Sweden, 2012. ISBN: 9789173857673.

[13] P.L. Gilabert, G. Montoro, D. Lopez, N. Bartzoudis, E. Bertran, M. Payaro, and A Hourtane. Order reduction of wideband digital predistorters using principal component analysis. In *Microwave Symposium Digest (IMS), 2013 IEEE MTT-S International*, pages 1–7, June 2013.

[14] I.T. Jolliffe. *Principal Component Analysis*. Springer, second edition, 2002. ISBN: 0387954422.